Coherence Analysis of Small Baseline Subset Displacement Model Types in Deformation Monitoring

Sefercik U.G.[1], Nazar M. [1*] and Gorken M.[2]

[1]Department of Geomatics Engineering, Faculty of Engineering, Gebze Technical University, Türkiye

[2]Architecture and Urban Planning, Land Registry and Cadastre Program, Şefaatli Vocational School, Yozgat Bozok University, Türkiye

*mnazar@gtu.edu.tr (*Corresponding author's email only)

Abstract: *In coastal cities around the globe, engineering projects for land reclamation are being implemented to accommodate the demands of rapid population growth and economic development. To provide the necessary transformation services, airports are constructed in a variety of reclaimed areas, including overly moist agricultural regions, oceans, seas, lakebeds, and riverbeds. Nevertheless, the process of land reclamation can give rise to subsidence phenomena, which may subsequently result in damage to the infrastructure and buildings. It is therefore imperative that deformation monitoring be conducted in reclaimed airports to prevent potential risks. In this context, the small baseline subset (SBAS) method, which is a multi-temporal interferometric synthetic aperture radar (MT-InSAR) approach, has been adopted in numerous studies and has subsequently become a valuable asset. Moreover, the utilization of the SBAS method facilitates the implementation of deformation time series analysis in the reclaimed airport areas. In this study, coherence analysis was conducted on two types of SBAS displacement models: linear and quad. The analysis was carried out by monitoring deformation in Hatay Airport with a dataset of Sentinel-1A single-look complex (SLC) SAR images, spanning the period between 2 December 2017 and 29 January 2023. Furthermore, atmospheric correction was conducted using the Generic Atmospheric Correction Online Service for InSAR (GACOS) data. In this context, both the average deformation velocity and the cumulative deformation were acquired in the satellite line-of-sight (LOS) direction. Additionally, the cumulative deformation in the vertical direction was obtained for the linear and quad SBAS displacement models, with values ranging from -142.71 mm to 60.11 mm and from -224.97 mm to 73.98 mm, respectively. Finally, the cumulative vertical deformation difference map of the linear and quad SBAS displacement models was generated, and a coherence analysis was conducted.*

Keywords: deformation monitoring, displacement model, multi-temporal synthetic aperture radar, reclamation area, small baseline subset

Introduction

Cities situated along coastlines across the globe are engaged in engineering projects aimed at reclaiming territory to accommodate accelerated population growth and economic expansion. In order to create new, buildable land from previously unsuitable areas, such as wetlands, coastal regions, and other bodies of water, it is necessary to alter the ground morphology (Martín-Antón et al., 2016). However, the process of land reclamation may result in subsidence and cracking due to the influence of a number of factors, which may potentially pose a significant risk to buildings and the well-being of the population (Shi et

al., 2023). In particular, reclaimed airport areas require the periodic investigation of ground deformation in order to mitigate disasters and sustain operational safety (Bao et al., 2022). A variety of methods are utilized for the detection of ground deformation induced by reclamation activities. Traditional methods for the monitoring of ground deformations are predominantly point-constrained, rendering them unsuitable for the observation of large areas, while also being costly, time-consuming, and exhibiting low temporal resolution (An et al., 2023). The utilization of remote sensing has emerged as a viable alternative for the detection of ground deformation. In comparison to traditional ground deformation monitoring methods, interferometric synthetic aperture radar (InSAR) is capable of providing sub-centimeter accuracy in the detection of deformation across extensive areas (Jiang et al., 2016). InSAR employs phase differences between successive SAR images acquired over a given area to generate interferograms (Lu et al., 2007; Osmanoglu et al., 2016; Sefercik et al., 2020). Furthermore, the differential InSAR (DInSAR) method, which employs the phase difference between at least two SAR images (repeat-pass, double-pass, multi-pass) captured by repeatedly passing through the target area to generate differential interferograms, can be employed to detect surface deformations with cm-mm accuracy (Hanssen, 2001; Kampes, 2006; Agram, 2010; Yonezawa et al., 2012). The limitations of the DInSAR method, including decorrelation, atmospheric difference sensitivity, and orbital variations, have prompted the proposal of multi-temporal InSAR (MT-InSAR) methods for the monitoring of time series of ground deformation in large areas (Massonnet & Feigl, 1998; Hooper, 2008; Cigna et al., 2011). A methodology based on MT-InSAR designated small baseline subset (SBAS) has been proposed as a means of reducing baseline decorrelation and increasing the temporal sampling rate through the utilization of an optimal combination of differential interferograms (Berardino et al., 2002). Furthermore, a variety of methods were developed for quantifying and mitigating the impact of the atmospheric phase contribution on interferogram quality. One example of an atmospheric phase correction method is the recently proposed Generic Atmospheric Correction Online Service for InSAR (GACOS), which is based on the utilization of an iterative tropospheric decomposition (ITD) model (Yu et al., 2017; Yu et al., 2018a; Yu et al., 2018b).

The objective of this study is to utilize coherence analysis to examine the performance of linear and quad SBAS displacement models in monitoring ground deformation at Hatay Airport. The analysis was based on 151 Sentinel-1A single-look complex (SLC) images

acquired between 2 December 2017 and 29 January 2023. Furthermore, the atmospheric phase was corrected using data from the GACOS.

Study Area and Dataset

The Hatay Airport is situated within the Hatay Province of Turkey at 36°21'46.0"N and 36°16'56.0"E. With an approximate total area of 2.70 km^2 and a total terminal area of 46826 m^2, Hatay Airport has a single concrete runway measuring 3000 x 45 meters. Hatay Airport was constructed on the site of the former Lake Amik, which had been desiccated, and it was officially inaugurated in 2007. The location of Hatay Airport is displayed in Figure 1.

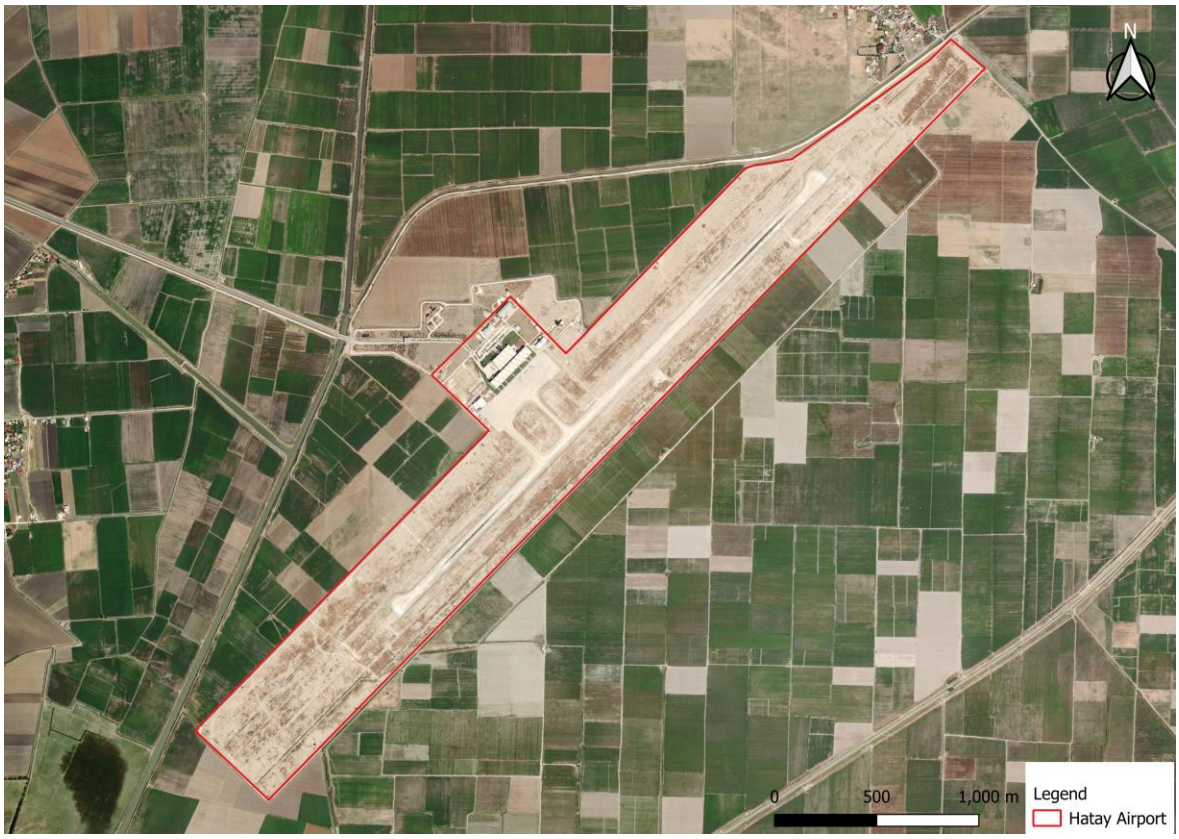

Figure 1: The location of Hatay Airport.

A dataset comprising 151 Sentinel-1A SLC SAR images in descending orbit acquired in interferometric wide swath (IW) mode between 2 December 2017 and 29 January 2023, was employed for the purpose of monitoring ground deformation at Hatay Airport. SAR images were acquired in vertical polarization (VV) from the Alaska Satellite Facility's

(ASF) Vertex Platform. The characteristics of the employed Sentinel-1A SLC dataset are outlined in Table 1.

Table 1: Features of the utilized UAV and TLS equipment.

Features	Description
Product type	Sentinel-1A TOPS SLC
Orbit direction	Descending
Polarization	VV
Acquisition mode	IW
Wavelength	C-band (5.55 cm)
Number of images	151
Acquisition date	20171202-20230129
Path/Frame No.	21/14
Spatial resolution	5 m (ground range) x 20 m (azimuth)
Pixel spacing	2.3 m (slant range) x 14.1 m (azimuth)
Revisit frequency	12 days
Incidence angle	29°-46°
Total swath width	250 km

Methodology

One of the MT-InSAR methods, SBAS, has the capacity to minimize spatial decorrelation and topographic errors based on the combination of differential interferograms with small baselines between them (Berardino et al., 2002). SBAS was initially developed for the analysis of deformations at a grid size of 100 x 100 m, which may prove inadequate for the analysis of deformations at finer scales. In a separate contribution, Lanari et al., (2004) proposed an alternative SBAS methodology for local-scale deformations based on a multilook and a single-look dataset. The SBAS method was demonstrated to have the capacity to discern average deformation velocities with standard deviations of 1 mm/year (Casu et al., 2006). The SBAS method was implemented in the SARscape 5.6.2.1 SAR processing software, which was executed within the ENVI 5.6.3 software suite. In summary, the working principle of SBAS is as follows: pixels in the images are matched according to a super master image. A multitude of differential interferograms are generated through a binary combination of the total number of images. The phase difference of these interferograms is then calculated. In order to ensure a high level of correlation, data generated with image pairs exhibiting a shorter temporal baseline than the others are selected. Subsequently, a singular value decomposition (SVD) approach based on linear algebra is applied to the targets exhibiting high coherence in these data,

with the objective of obtaining the deformation rate (Casagli et al., 2016). SBAS appears to yield superior outcomes in open settings, thereby making it a prevalent choice for the detection and monitoring of surface alterations and land subsidence, particularly in urban areas (Dehghani et al., 2009; Zhao et al., 2011; Sun et al., 2015; Novellino et al., 2017; Zhang et al., 2019). Furthermore, it is employed for the identification and examination of deformations resulting from landslides (Castañeda et al., 2009; Liu et al., 2013; Huang Lin et al., 2019; Dong et al., 2018), mining operations (Gourmelen et al., 2007; Baek et al., 2008; Choi et al., 2011; Grzovic & Ghulam, 2015), volcanic activities (Lanari et al., 2007; Stramondo et al., 2008), and earthquakes (Guzzetti et al., 2009; Salvi et al., 2012; Jebur et al., 2015). The SBAS processing for this study was applied through steps according to the SARscape SBAS tutorial manual (version 5.6.2) (SARMAP, 2022). These include connection graph, optimal master selection, coregistration and initial phase unwrapping, refinement and flattening, first inversion, second inversion, atmospheric correction using GACOS data, and geocoding process. The super master image was selected as the image with the date 12 August 2020 and all other slave images were coregistered according to the master. The atmospheric correction process was achieved using GACOS data on the same dates as the Sentinel-1A SLC dataset. In order to obtain cumulative vertical deformation, a three-dimensional decomposition of the displacement vector was conducted in accordance with the methodology set forth by Hanssen (2001) in Equation 1.

$$d_r = d_u \cos(\theta_{inc}) - \sin(\theta_{inc}) \left[d_n \cos\left(\alpha_h - \frac{3\pi}{2}\right) + d_e \sin\left(\alpha_h - \frac{3\pi}{2}\right) \right] \quad (1)$$

In the aforementioned equation, d_r represents the slant-range component in the line-of-sight (LOS) direction, d_n denotes the component in the north-south direction, d_e signifies the component in the east-west direction, and d_u is the component in the up-down direction of a three-dimensional (3D) displacement vector $\vec{d}$, θ_{inc} is the incidence angle and α_h is the satellite heading angle. In the absence of any north-south or east-west movement, the vertical deformation in the up-down direction was calculated in accordance with Equation 2.

$$d_u = \frac{d_r}{\cos(\theta_{inc})} \quad (2)$$

Results and Discussion

The data visualization and map generation were performed using the QGIS 3.32.3 software. Average LOS deformation velocity and cumulative LOS deformation maps of linear and quad SBAS displacement models are shown in Figure 2.

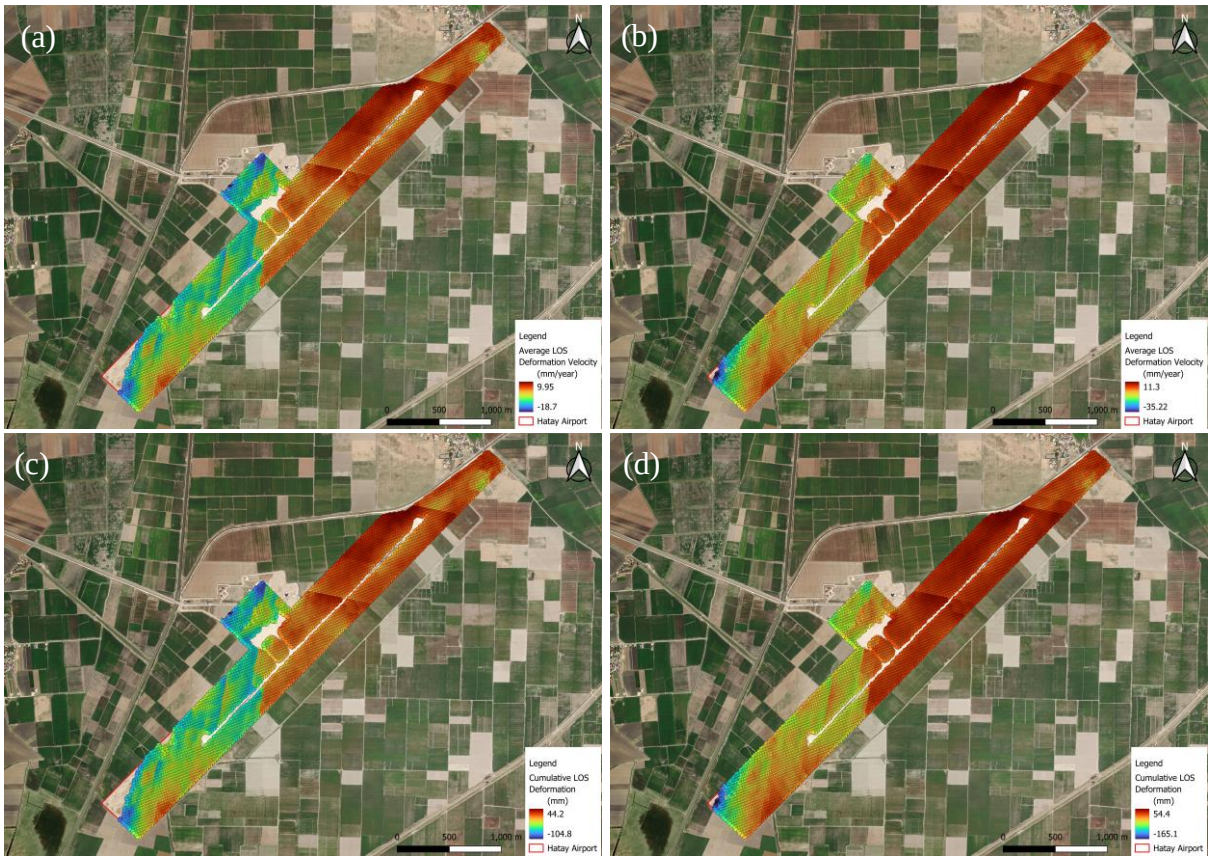

Figure 2: Average LOS deformation velocity maps for (a) linear and (b) quad SBAS displacement models and cumulative LOS deformation maps for (c) linear and (d) quad SBAS displacement models.

The average LOS deformation velocities for the linear and quad SBAS displacement models were found to be between -18.7 mm/year and 9.95 mm/year, and between -35.22 mm/year and 11.3 mm/year, respectively. The cumulative LOS deformations for the linear and quad SBAS displacement models were observed to range between -104.8 mm and 44.2 mm, and between -165.1 mm and 54.4 mm, respectively. The total number of scatter points for the linear and quad SBAS models was 11244 and 11581, respectively. The average LOS velocities and cumulative LOS deformations for both displacement models were observed to move closer to the satellite sensor on the northern side, in contrast to the southern side, where they were observed to move away from the satellite sensor. The density of points was

markedly diminished in the runway and terminal area in comparison to the remainder of the site. Cumulative vertical deformation maps of linear and quad SBAS displacement models are shown in Figure 3.

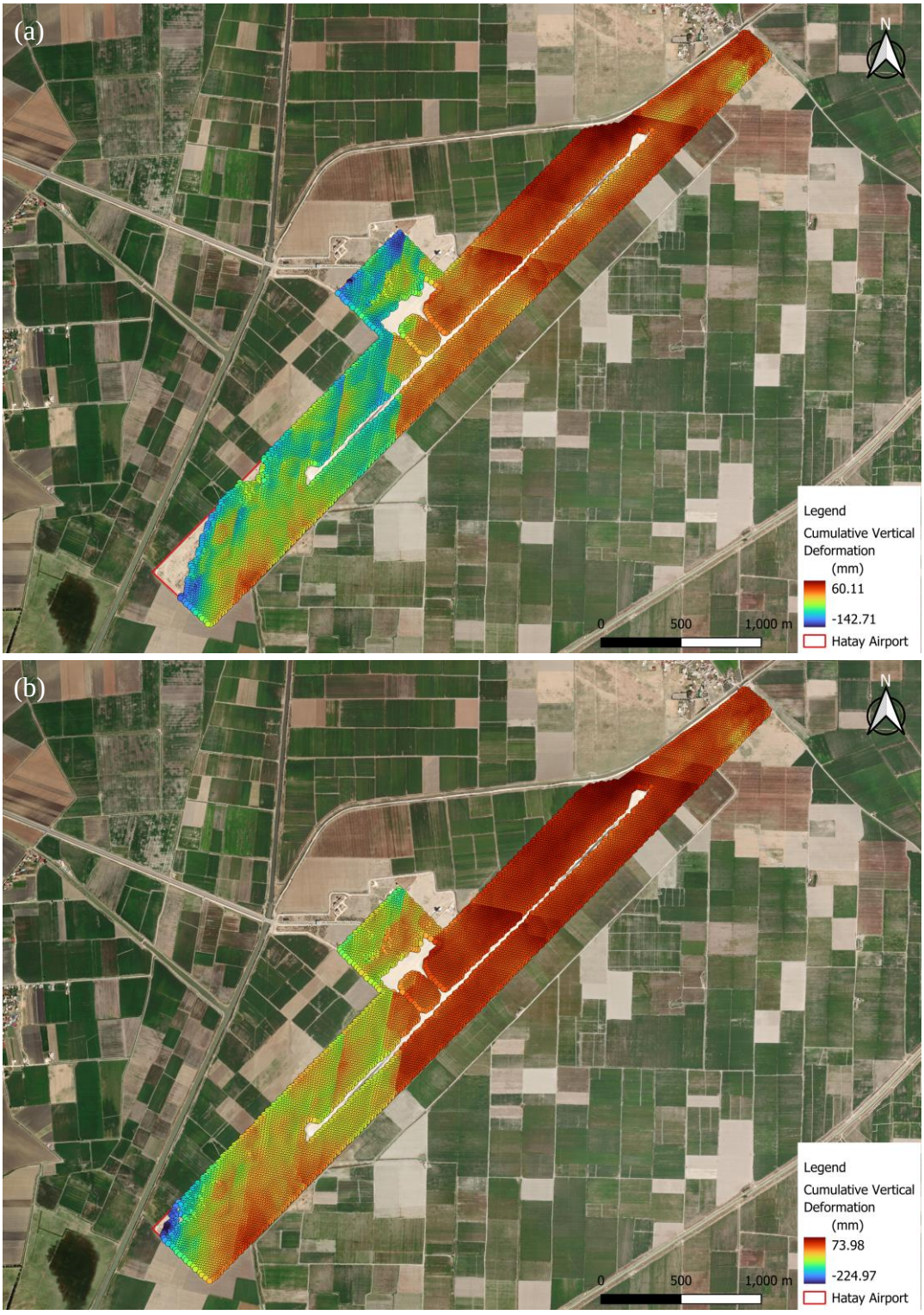

Figure 3: Cumulative vertical deformation maps of linear (a) and quad (b) SBAS displacement models.

The cumulative vertical deformation values for the linear and quad SBAS displacement models ranged from -142.71 to 60.11 mm and from -224.97 to 73.98 mm, respectively. A vector-to-raster transformation was applied in Surfer software to points with cumulative vertical deformation values using the nearest neighbor interpolation method and a grid spacing of 5 m. Subsequently, a coherence analysis of the cumulative vertical deformation maps of linear and quad SBAS displacement models in raster format was conducted in BLUH (Bundle Block Adjustment Leibniz University Hannover) software, employing the standard deviation metric. The total number of pixels for the linear and quad SBAS displacement models were 87940 and 90485, respectively. The results of the coherence analysis of the linear and quad SBAS displacement models are presented in Table 2.

Table 2: The results of the coherence analysis of the linear and quad SBAS displacement models (REF=Reference model, CM= Compared model, EB= Eliminated bias).

Standard deviation (mm)		
CM \ REF	Linear	Quad
Linear	0.000	8.316 (EB= 13.512)
Quad	8.316 (EB= -13.512)	0.000

The frequency and standard deviation histogram of the differences between the cumulative vertical deformation values of the linear and quad SBAS displacement models are presented in Figure 4.

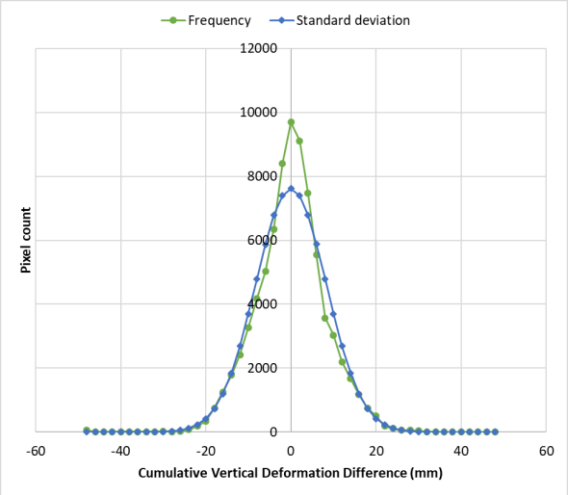

Figure 4: The frequency and standard deviation histogram of the differences between the cumulative vertical deformation values of the linear and quad SBAS displacement models.

The cumulative vertical deformation difference map of linear and quad SBAS displacement models is presented in Figure 5.

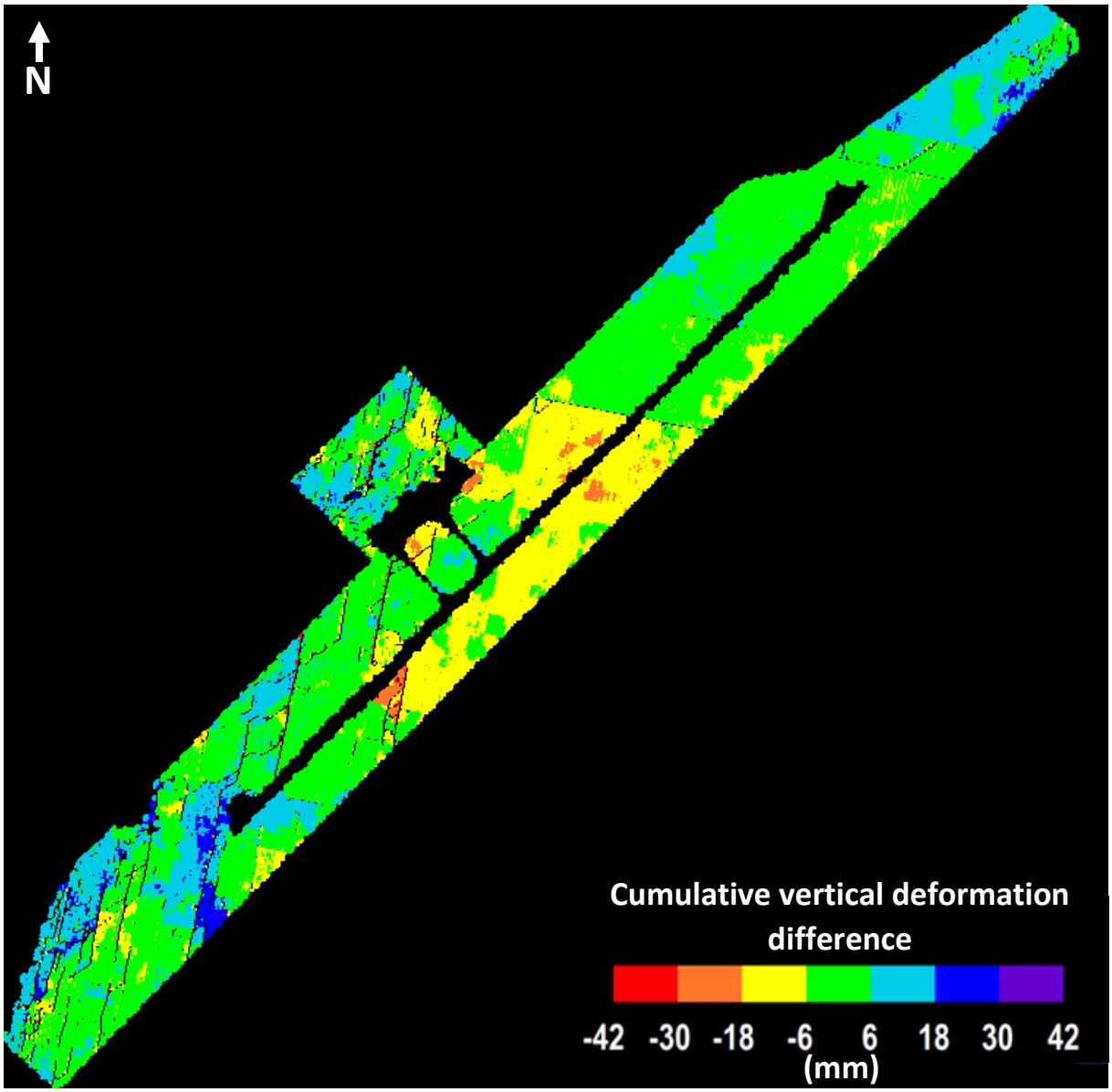

Figure 5: The cumulative vertical deformation difference map of linear and quad SBAS displacement models.

The cumulative vertical deformation difference was observed to range between -42 mm and 42 mm. Nevertheless, the cumulative vertical deformation differences for both the linear and quad SBAS displacement models were predominantly observed to be at a maximum of ±18 mm.

Conclusion and Recommendation

The construction of an airport in reclaimed areas may result in the airport becoming susceptible to subsidence and infrastructural damage. It is therefore imperative to monitor ground deformation in order to guarantee the uninterrupted operation of airports and the safety of the general public. In addition to the traditional terrestrial methods, the InSAR method is employed for the monitoring of ground deformation at the millimeter level. A MT-InSAR method, designated SBAS, is employed for the periodic detection of ground deformation induced by reclamation in airport areas. The present study employed coherence analysis of linear and quad SBAS displacement models for the purpose of monitoring ground deformation at Hatay Airport. In order to achieve this objective, 151 Sentinel-1A SLC SAR images, obtained between 2 December 2017 and 29 January 2023, were employed for the purpose of detecting ground deformation in an airport area that had been subject to reclamation. The average LOS deformation velocity for the linear and quad SBAS displacement models was found to be between -18.7 mm/year and 9.95 mm/year, and between -35.22 mm/year and 11.3 mm/year, respectively. The cumulative LOS deformation for the linear and quad SBAS displacement models was observed to range between -104.8 mm and 44.2 mm, and between -165.1 mm and 54.4 mm, respectively. The cumulative vertical deformation for the linear and quad SBAS displacement models was calculated to be between -104.8 mm and -44.2 mm, and between -165.1 mm and -54.4 mm, respectively. A vector-to-raster transformation was employed for the purpose of conducting a coherence analysis of cumulative vertical deformation maps of both linear and quad SBAS displacement models. Following the elimination of bias, the standard deviation of differences in cumulative vertical deformation values was 8.316 mm. A cumulative vertical deformation difference map of linear and quad SBAS displacement models was generated, with values ranging between -42 mm and 42 mm. In the vicinity of the airport, the maximum cumulative vertical deformation difference was mostly ±18 mm. While the differences in cumulative vertical deformation observed between the linear and quad SBAS displacement models were less than one centimeter in certain areas, there were instances where these discrepancies were more pronounced. It has been demonstrated that the selection of a displacement model can influence the outcomes of deformation monitoring in the context of reclaimed airport areas. The SBAS method demonstrates promise for the monitoring of deformation in reclaimed airports, with the potential to facilitate hazard mitigation and enhance safety. Furthermore, the results of SBAS deformation monitoring can be employed in a wider context to facilitate the identification

of potential risks and the evaluation of the structural safety of engineering structures in reclaimed areas.

References

Agram, P. S. (2010). Persistent Scatterer Interferometry in Natural Terrain. Doctoral dissertation, Stanford University, California, USA, 163.

An, B., Jiang, Y., Wang, C., Shen, P., Song, T., Hu, C., & Liu, K. (2023). Ground Infrastructure Monitoring in Coastal Areas Using Time-Series inSAR Technology: The Case Study of Pudong International Airport, Shanghai. *International Journal of Digital Earth, Volume 16(1), 355-374.*

Baek, J., Kim, S. W., Park, H. J., Jung, H. S., Kim, K. D., & Kim, J. W. (2008). Analysis of Ground Subsidence in Coal Mining Area Using SAR Interferometry. *Geosciences Journal, Volume 12, 277-284.*

Bao, X., Zhang, R., Shama, A., Li, S., Xie, L., Lv, J., Fu, Y., Wu, G., & Liu, G. (2022). Ground Deformation Pattern Analysis and Evolution Prediction of Shanghai Pudong International Airport Based On PSI Long Time Series Observations. *Remote Sensing, Volume 14(3), 610.*

Berardino, P., Fornaro, G., Lanari, R., & Sansosti, E. (2002). A New Algorithm for Surface Deformation Monitoring Based On Small Baseline Differential SAR Interferograms. *IEEE Transactions On Geoscience and Remote Sensing, Volume 40(11), 2375-2383.*

Casagli, N., Cigna, F., Bianchini, S., Hölbling, D., Füreder, P., Righini, G., Del Conte, S., Friedl, B., Schneiderbauer, S., Iasio, C., & Vlcko, J. (2016). Landslide Mapping and Monitoring by Using Radar and Optical Remote Sensing: Examples from The EC-FP7 Project SAFER. *Remote Sensing Applications: Society and Environment, Volume 4, 92-108.*

Castañeda, C., Gutiérrez, F., Manunta, M., & Galve, J. P. (2009). DInSAR Measurements of Ground Deformation by Sinkholes, Mining Subsidence, And Landslides, Ebro River, Spain. *Earth Surface Processes and Landforms, Volume 34(11), 1562-1574.*

Casu, F., Manzo, M., & Lanari, R. (2006). A Quantitative Assessment of The SBAS Algorithm Performance for Surface Deformation Retrieval from DInSAR Data. *Remote Sensing of Environment, Volume 102(3-4), 195-210.*

Choi, J. K., Won, J. S., Lee, S., Kim, S. W., Kim, K. D., & Jung, H. S. (2011). Integration of A Subsidence Model and SAR Interferometry for A Coal Mine Subsidence Hazard Map in Taebaek, Korea. *International Journal of Remote Sensing, Volume 32(23), 8161-8181.*

Cigna, F., Del Ventisette, C., Liguori, V., & Casagli, N. (2011). Advanced Radar-Interpretation of InSAR Time Series for Mapping and Characterization of Geological Processes. *Natural Hazards and Earth System Sciences, Volume 11(3), 865-881.*

Dehghani, M., Valadan Zoej, M. J., Entezam, I., Mansourian, A., & Saatchi, S. (2009). InSAR Monitoring of Progressive Land Subsidence in Neyshabour, Northeast Iran. *Geophysical Journal International, Volume 178(1), 47-56.*

Dong, J., Liao, M., Xu, Q., Zhang, L., Tang, M., & Gong, J. (2018). Detection and Displacement Characterization of Landslides Using Multi-Temporal Satellite SAR Interferometry: A Case Study of Danba County in The Dadu River Basin. *Engineering Geology, Volume 240, 95-109.*

Gourmelen, N., Amelung, F., Casu, F., Manzo, M., & Lanari, R. (2007). Mining-Related Ground Deformation in Crescent Valley, Nevada: Implications for Sparse GPS Networks. *Geophysical Research Letters, Volume 34(9).*

Grzovic, M., & Ghulam, A. (2015). Evaluation of Land Subsidence from Underground Coal Mining Using TimeSAR (SBAS and PSI) In Springfield, Illinois, USA. *Natural Hazards, Volume 79, 1739-1751.*

Guzzetti, F., Manunta, M., Ardizzone, F., Pepe, A., Cardinali, M., Zeni, G., Reichenbach, P., & Lanari, R. (2009). Analysis of Ground Deformation Detected Using The SBAS-DInSAR Technique in Umbria, Central Italy. *Pure and Applied Geophysics, Volume 166, 1425-1459.*

Hanssen, R. F. (2001). Radar Interferometry Data Interpretation and Error Analysis. Kluwer Academic Publisher, Dordrecht, The Netherlands, 327.

Hanssen, R. F. (2001). Radar Interferometry: Data Interpretation and Error Analysis. Kluwer Academic Publishers, Dordrecht, The Netherlands.

Hooper, A. (2008). A Multi-Temporal InSAR Method Incorporating Both Persistent Scatterer and Small Baseline Approaches. *Geophysical Research Letters, Volume 35(16).*

Huang Lin, C., Liu, D., & Liu, G. (2019). Landslide Detection in La Paz City (Bolivia) Based On Time Series Analysis of InSAR Data. *International Journal of Remote Sensing, Volume 40(17), 6775-6795.*

Jebur, M. N., Pradhan, B., & Tehrany, M. S. (2015). Using ALOS PALSAR Derived High-Resolution DInSAR to Detect Slow-Moving Landslides in Tropical Forest: Cameron Highlands, Malaysia. *Geomatics, Natural Hazards and Risk, Volume 6(8), 741-759.*

Jiang, Y., Liao, M., Wang, H., Zhang, L., & Balz, T. (2016). Deformation Monitoring and Analysis of the Geological Environment of Pudong International Airport with Persistent Scatterer SAR Interferometry. *Remote Sensing, Volume 8(12), 1021.*

Kampes, B. M. (2006). The Permanent Scatterer Technique. Radar Interferometry: Persistent Scatterer Technique. Springer-Verlag, Dordrecht, The Netherlands, 12, 5-30.

Lanari, R., Casu, F., Manzo, M., Zeni, G., Berardino, P., Manunta, M., & Pepe, A. (2007). An Overview of the Small Baseline Subset Algorithm: A Dinsar Technique for Surface Deformation Analysis. *Deformation and Gravity Change: Indicators of Isostasy, Tectonics, Volcanism, and Climate Change, 637-661.*

Lanari, R., Mora, O., Manunta, M., Mallorquí, J. J., Berardino, P., & Sansosti, E. (2004). A Small-Baseline Approach for Investigating Deformations On Full-Resolution Differential SAR Interferograms. *IEEE Transactions On Geoscience and Remote Sensing, Volume 42(7), 1377-1386.*

Liu, P., Li, Z., Hoey, T., Kincal, C., Zhang, J., Zeng, Q., & Muller, J. P. (2013). Using Advanced InSAR Time Series Techniques to Monitor Landslide Movements in Badong of

the Three Gorges Region, China. *International Journal of Applied Earth Observation and Geoinformation, Volume 21, 253-264.*

Lu, Z., Kwoun, O., & Rykhus, R. (2007). Interferometric Synthetic Aperture Radar (InSAR): Its Past, Present and Future. *Photogrammetric engineering and remote sensing, Volume 73(3), 217.*

Martín-Antón, M., Negro, V., del Campo, J. M., López-Gutiérrez, J. S., & Esteban, M. D. (2016). *Review of Coastal Land Reclamation Situation in The World. Journal of Coastal Research, Volume 75, 667-671.*

Massonnet, D., & Feigl, K. L. (1998). Radar Interferometry and Its Application to Changes in The Earth's Surface. *Reviews of Geophysics, Volume 36(4), 441-500.*

Novellino, A., Cigna, F., Brahmi, M., Sowter, A., Bateson, L., & Marsh, S. (2017). Assessing The Feasibility of a National InSAR Ground Deformation Map of Great Britain with Sentinel-1. *Geosciences, Volume 7(2), 19.*

Osmanoğlu, B., Sunar, F., Wdowinski, S., & Cabral-Cano, E. (2016). Time Series Analysis of InSAR Data: Methods and Trends. *ISPRS Journal of Photogrammetry and Remote Sensing, Volume 115, 90-102.*

Salvi, S., Atzori, S., Tolomei, C., Antonioli, A., Trasatti, E., Boncori, J. M., Pezzo, G., Coletta, A., & Zoffoli, S. (2012). Results from INSAR Monitoring of The 2010–2011 New Zealand Seismic Sequence: EA Detection and Earthquake Triggering. *IEEE International Geoscience and Remote Sensing Symposium, 22-27 July 2012, Munich, Germany, 3544-3547.*

SARMAP. (2022). SARscape SBAS Tutorial Manual (Version 5.6.2). Available online: https://www.sarmap.ch/tutorials/SBAS_Tutorial_562.pdf.

Sefercik, U. G., Buyuksalih, G., & Atalay, C. (2020). DSM Generation with Bistatic Tandem-X InSAR Pairs and Quality Validation in Inclined Topographies and Various Land Cover Classes. *Arabian Journal of Geosciences, Volume 13, 560.*

Shi, X., Zhong, J., Yin, Y., Chen, Y., Zhou, H., Wang, M., & Dai, K. (2023). Integrating SBAS-InSAR and LSTM for Subsidence Monitoring and Prediction at Hong Kong International Airport. *Ore and Energy Resource Geology, Volume 15, 100032.*

Stramondo, S., Bozzano, F., Marra, F., Wegmuller, U., Cinti, F. R., Moro, M., & Saroli, M. (2008). Subsidence Induced by Urbanisation in The City of Rome Detected by Advanced InSAR Technique and Geotechnical Investigations. *Remote Sensing of Environment, Volume 112(6), 3160-3172.*

Sun, Q., Zhang, L., Ding, X. L., Hu, J., Li, Z. W., & Zhu, J. J. (2015). Slope Deformation Prior to Zhouqu, China Landslide from InSAR Time Series Analysis. *Remote Sensing of Environment, Volume 156, 45-57.*

Yonezawa, C., Watanabe, M., & Saito, G. (2012). Polarimetric Decomposition Analysis of ALOS PALSAR Observation Data Before and After a Landslide Event. *Remote Sensing, Volume 4(8), 2314-2328.*

Yu, C., Li, Z., & Penna, N. T. (2018a). Interferometric Synthetic Aperture Radar Atmospheric Correction Using A GPS-Based Iterative Tropospheric Decomposition Model. *Remote Sensing of Environment, Volume 204, 109-121.*

Yu, C., Li, Z., Penna, N. T., & Crippa, P. (2018b). Generic Atmospheric Correction Model for Interferometric Synthetic Aperture Radar Observations. *Journal of Geophysical Research: Solid Earth, Volume 123(10), 9202-9222.*

Yu, C., Penna, N. T., & Li, Z. (2017). Generation of Real-Time Mode High-Resolution Water Vapor Fields from GPS Observations. *Journal of Geophysical Research: Atmospheres, Volume 122(3), 2008-2025.*

Zhang, Y., Liu, Y., Jin, M., Jing, Y., Liu, Y., Liu, Y., Sun, W., Wei, J., & Chen, Y. (2019). Monitoring Land Subsidence in Wuhan City (China) Using The SBAS-InSAR Method with Radarsat-2 Imagery Data. *Sensors, Volume 19(3), 743.*

Zhao, C. Y., Zhang, Q., Yang, C., & Zou, W. (2011). Integration of MODIS Data and Short Baseline Subset (SBAS) Technique for Land Subsidence Monitoring in Datong, China. *Journal of Geodynamics, Volume 52(1), 16-23.*